University of Wollongong

Research Online

1-1-2016

Elastomeric and dynamic MnO2/CNT core-shell structure coiled yarn supercapacitor

Changsoon Choi
Hanyang University

Hyeon Jun Sim
Hanyang University

Geoffrey M. Spinks
University of Wollongong, gspinks@uow.edu.au

Xavier Lepró
University of Texas

Ray H. Baughman
University of Texas, ray.baughman@utdallas.edu

See next page for additional authors

Follow this and additional works at: https://ro.uow.edu.au/eispapers

Recommended Citation

Elastomeric and dynamic MnO2/CNT core-shell structure coiled yarn supercapacitor

Abstract

Reversibly deformable and highly performing solid-state yarn supercapacitors are obtained using MnO2-deposited microcoiled yarn electrodes. The core(CNT)-shell(MnO2)-structured coiled electrodes achieve high stretchability (37.5%) without the help of elastomeric substrates, minimizing the size of the supercapacitors. Therefore, high specific capacitances of 34.6 F cm−3, 61.25 mF cm−2, and 2.72 mF cm−1 are achieved for coiled supercapacitors without impairing mechanical stretchability or electrochemical cyclability.

Disciplines

Engineering | Science and Technology Studies

Publication Details

Authors

Changsoon Choi, Hyeon Jun Sim, Geoffrey M. Spinks, Xavier Lepró, Ray H. Baughman, and Seon Jeong Kim

Elastomeric and Dynamic MnO₂/CNT Core-Shell Structure Coiled Yarn Supercapacitor

Changsoon Choi, Hyeon Jun Sim, Geoffrey M. Spinks, Xavier Lepro, Ray H. Baughman and Seon Jeong Kim*

C. Choi, H. J. Sim, Prof. S. J. Kim

Center for Self-powered Artificial Muscle and Department of Biomedical Engineering,

Hanyang University, Seoul 133-791, Korea, [*] E-mail: sjk@hanyang.ac.kr

Prof. G. M. Spinks,

Intelligent Polymer Research Institute, ARC Centre of Excellence for Electromaterials

Science, University of Wollongong, Wollongong, NSW 2522, Australia.

Dr. X. Lepro, Prof. R. H. Baughman

The Alan G. MacDiarmid Nano Tech Institute, University of Texas at Dallas, Richardson, TX,

75083, USA.

One-dimensional (1-D) yarn/fiber supercapacitors are more attractive power sources than conventional three- or two-dimensional (3-D, 2-D) foam/film-type when they are used for miniaturized electronic devices, textile electronics, and implantable medical devices[1] because their small volume and high flexibility enable them to be easily integrated into the devices with a tiny size and various shapes. Nevertheless, most fiber-based supercapacitors (FBSs) simply possess the flexibility with limited tensile strain and stretchability[2–16] because they are mostly based on nonstretchable electrodes such as carbon nanotube (CNT) spun yarn,[2–7] graphene fiber,[8–12] carbon fiber,[13,14] and metal wire.[15] This lack of stretchability of these FBSs leads to limitation for more advanced utilization, e.g., as a power source for artificial muscles[17] or wearable devices that are exposed to high strain, especially in the joint part.[18] In recent years, several strategies have been reported to incorporate stretchability into FBSs: CNT sheet nanomembranes were wound onto elastic fibers to make highly stretchable FBSs[19-21] or CNT fiber electrodes were attached onto prestrained elastic fibers to form a micro-buckling structure for FBSs.[22,23] Although these FBSs exhibited stable stretchability and energy storage performances, they still suffer from low electrochemical energy storage performance because the additional core fibers used as elastomeric substrates do not participate in electrochemical energy storage reactions but merely provide stretchability, resulting in low gravimetric and volumetric energy storage performances of the total devices.[24] To solve these problems, novel spring-like stretchable CNT fibers were proposed as supercapacitor electrodes.[24] It is notable that stretchability could be achieved for the first time in FBSs by using the spring CNT fiber without the help of any elastomeric substrate. However, the spring-based supercapacitors still showed limited capacitances because their active material was based on pristine CNT, totally depending on the electrochemical double layer capacitance (EDLC) energy storage mechanism. All things considered, achieving FBSs

possessing not only stretchability but also excellent specific capacitances remains challenging.

In this study, we present coil structured, pseudocapacitive yarns as promising electrodes for achieving stretchable and highly performing supercapacitors. The bare CNT coiled yarns are fabricated by inserting a giant twist (50,000 twists/m) into CNT spun yarns, which are drawn from a multiwalled carbon nanotube (MWNT) forest.[25] Although the bare CNT coiled yarns can be used as stretchable electrodes for EDLC-based supercapacitor without further processing,[24] we deposited MnO_2, which is a promising pseudocapacitive material because of its high theoretical capacitance, low cost, and environmental friendliness[26] to enhance dramatically its energy storage capacity. A scanning electron microscope (SEM) image of the our novel core(CNT)–shell(MnO_2) structured hybrid coiled yarn is shown in **Figure 1**A. The diameter of the single hybrid coiled electrode is ~80 μm and about 200 uniform microloops are contained in a centimeter of coiled electrode. The resulting aspect ratio (ratio of coiled electrode's length to diameter) is high (about 210) and the electrode volume is impressively small (~ 6.5×10^{-5} cm^3) that the volume of presented coiled CNT electrode is one-twentieth the size of previously reported coiled CNT/nylon fiber[21].

A high-resolution SEM surface image of the bare CNT coiled yarn (Figure 1B) shows closely packed and uniaxially aligned CNT bundles, which implies an effective electron pathway for longitudinal current collecting. After the MnO_2 deposition (Figure 1C), a mesoporous film, which is morphologically characteristic of MnO_2,[27] is uniformly formed on the surface of the coiled electrode. It is experimentally confirmed that strong adhesion of the MnO_2 thin shell to the porous CNT surface is achieved so that high electrochemical stability could be demonstrated against repeated mechanical deformation by loop opening or electrochemical reaction, which will be discussed later. In this study, the mass of MnO_2 was

3

measured using an electrochemical quartz-crystal microbalance (EQCM). From the slope of the charge–mass graph measured by EQCM, the mass of MnO_2 per unit charge transferred during deposition is determined to be 5.4×10^{-4} g C^{-1}, as shown in **Figure S1**. To measure the thickness of the MnO_2 shell layer, cross-sectional analysis was performed by cutting the hybrid coiled electrode along its diameter using a Ga ion beam, as shown in Figure 1D. Figure 1E shows a magnified SEM image of the denoted rectangle at the edge part of the hybrid coiled yarn cross-section shown in Figure 1D. The nanoscopic MnO_2 shell with thickness ~1 μm is distinguished from the CNT core part. Because only nanoscopic surfaces of MnO_2 can participate in the electrochemical energy storage reaction, the loading amount of MnO_2 is controlled by adjusting its deposition time to have a thin shell with reasonable thickness (~1 μm) to obtain high capacitances and high-rate capability, simultaneously. As a consequence, volume and weight fractions of presented MnO_2 shell to total hybrid coiled electrode are calculated to be 4.9% and 17.2%, respectively. This pseudocapacitive micro-shell plays crucial role in enhancing energy storage performances of yarn supercapacitors.

Energy dispersive spectroscopy (EDS) analysis was performed to characterize clearly the hybrid core–shell structure of the electrode. Elemental mapping analysis for C, O, and Mn atoms was performed on the Figure 1D image to detect the location of specific atoms, as shown in **Figure 2A**–C. The core part of the hybrid coiled electrode has highly densified CNT without any observable pores. This pure CNT core is well distinguished by dominant C atoms' detection (denoted by red dots, Figure 2A) while the shell part is mainly detected by O atoms (green dots, Figure 2B) and Mn atoms (blue dots, Figure 2C). Clearer identification of atomic core–shell structure can be confirmed through the overlapped C, O, Mn mapping images (**Figure S2**). Figure 2D indicates X-ray photoelectron spectroscopy (XPS) analysis of the deposited MnO_2 film. The binding energy difference between Mn $2p_{3/2}$ and Mn $2p_{1/2}$

4

peaks is about 11.8 eV, which exactly matches the value for MnO_2.[28] Therefore, it can be concluded that this nonvacuum-based, scalable, and cost-effective electrochemical deposition technique achieves successful core–shell structure formation for stretchable, pseudocapacitive yarn electrodes.

Figure 3A schematically illustrates the configuration of a complete solid-state, stretchable, and highly performing coiled supercapacitor. Two symmetric pseudocapacitive coiled electrodes were assembled in a parallel direction with constant gap and coated with aqueous poly(vinyl alcohol) (PVA)-based gel containing lithium chloride (LiCl) with thickness around 20 μm. Figure 3B shows cyclic voltammogram (CV) curves of bare coiled CNT and MnO_2/CNT core–shell coiled electrodes. Although the MnO_2 content is relatively small compared with the total electrode (4.9% volume fraction or 17.2% weight fraction), it achieves about 512% capacitance enhancement by the pseudocapacitive effect. Figure 3C shows CV curves of the solid-state coiled yarn supercapacitor measured with scan rates from 10 to 100 mV s^{-1}. The box-like rectangular-shaped CV curves without any redox peak well represent the pseudocapacitive characteristics of our coiled supercapacitor. The rectangular-shaped CV curves could be retained for high scan rates up to 500 mV s^{-1} (**Figure S3**), showing high-rate capability. Figure 3D shows the Nyquist curve of the coiled supercapacitor. A vertical curve indicates an excellent capacitive characteristic of the coiled supercapacitor. Moreover, low equivalent series resistance (ESR) as small as 0.07 Ω cm^3 is achieved (inset of Figure 3D). To inspect the charge/discharge characteristic of the coiled supercapacitor, galvanostatic curves at current densities of 0.2, 0.6, and 2 A cm^{-3} were measured (**Figure S4**). Symmetrical triangle-shaped galvanostatic curves show good agreement with Nyquist analysis, indicating the excellent pseudocapacitive characteristics of the coiled supercapacitor. The specific capacitances based on single electrode were calculated from the CV curves as

5

shown in Figure 3E. High volumetric capacitance (C_V, 34.6 F cm^{-3}), areal capacitance (C_A, 61.25 mF cm^{-2}), and linear capacitance (C_L, 2.72 mF cm^{-1}) could be achieved at 10 mV s^{-1} scan rate. The gravimetric capacitance (C_M) can be calculated about 26.5 F g^{-1} for the coiled supercapacitor. Dimensions of the total electrodes (both MnO$_2$/CNT coiled yarns) were used for normalization of specific capacitance. Moreover, high volumetric and areal energy densities (2.4 mWh/cm^3 and 8.5 µWh/cm^2) were achieved in our stretchable fiber supercapacitor. The maximum capacitance values at 10 mV s^{-1} are retained to about 71.6% at 100 mV s^{-1} and 39% at 500 mV s^{-1}, showing high-rate capability (Figure S3).

Specific capacitances of the coiled supercapacitors are compared with other FBSs in Table 1. Notably, the coiled supercapacitor exhibited much higher linear and areal capacitances (2.72 mF cm^{-1}, 61.25 mF cm^{-2}) than reported stretchable FBSs based on buckled CNT fiber (0.26 mF cm^{-1}, 27.98 mF cm^{-2})[23] and CNT spring fiber (0.51 mF cm^{-1}, 27.07 mF cm^{-2})[24] as shown in Table 1. It should be noted that the volumetric capacitance of the presented coiled supercapacitor (34.6 F cm^{-3}) was also excellent that about 10 times higher than our previous research on nylon fiber based stretchable supercapacitor (3.8 F cm^{-3})[21] without sacrificing linear and areal capacitances. These high specific capacitances were originated from effectively minimized volume of pristine CNT based coiled fibers (only 5.2% volume of previous stretchable fiber)[21] by not using any elastomeric substrates. Moreover, the observed specific capacitances are remarkably higher than other reported hybrid FBSs, which do not offer the benefits of reversible elastomeric deformability. For example, the volumetric capacitance of our coiled supercapacitor (34.6 F cm^{-3}) is about 14 times higher than MnO$_2$/carbon FBS (2.5 F cm^{-3})[13] and 7 times higher than MoS$_2$-reduced graphene oxide/CNT FBS (4.8 F cm^{-3})[7]. Moreover, its linear capacitance (2.72 mF cm^{-1}) is two orders higher than MnO$_2$/CNT FBS (0.019 mF cm^{-1})[2], MnO$_2$/ZnO nanowire-coated FBS (0.02 mF cm^{-1})[13] and

also significantly higher than CNT/reduced graphene oxide fiber (0.35 mF cm^{-1})[11]. Such high specific capacitances of our coiled supercapacitor compared with other FBSs can be attributed to the following two aspects. The first is that nanoscopic, mesoporous, and pseudocapacitive metal oxide coating effectively enables high energy storage performance, without sacrificing the high-rate capability or mechanical stretchability. Second, neither additional elastomeric substrate nor separator is used in our coiled supercapacitor system, dramatically minimizing the total dimension of the electrodes.

Figure 4A shows optical images of the complete coiled supercapacitor before and after 37.5% strain was applied. Although the theoretical maximum strain is much higher for coiled CNT yarn (about more than 300% strain, which originates from the relation L(coiled yarn length) $\approx l$(initial yarn length)$/\pi$),[29] we present 37.5% as the maximum strain for a coiled supercapacitor. Because the applied strain rate for static tests in this study is much faster (180 mm min^{-1} or 2% s^{-1}) than the literature [29] (0.5 mm min^{-1} strain rate, 15 minute intermediate stress relaxation every strain increment) that not enough relaxation time is provided to uniformly relax the generated internal stresses during stretching and this results in early fracture for the coiled yarn (~40% in tensile strain). In spite of such an early fracture, we adopted high strain rates (2–6% s^{-1} or 180–540 mm min^{-1} for dynamic tests) based stretching tests to reflect the real circumstances of wearable applications. The size of the tested supercapacitor was so small that it looks like a thin single thread to the naked eye, as shown in Figure 4A. Mechanical strain loading/unloading cycles were performed by applying tensile strains from 20% to 40% with sequentially 5% increments to the hybrid coiled electrode (Figure 4B). It is notable that the coiled electrode can be stretched up to 40% and reversibly recovered without significant residual deformation (less than 2.5%). This stretchable electrode's mechanical reversibility has not been reported among other stretchable FBSs.[19–24]

In addition, the constant slopes of the loading curves exhibit high modulus from 290 ($\varepsilon =$ 20%) to 325 MPa ($\varepsilon = 40\%$), while hysteretic energy dissipations by the recovery friction force were observed during unloading.[29] The capacitance retention of the coiled supercapacitor under mechanically static strain (2% s^{-1}) is characterized by comparing its CV curves before and after 37.5% strain was applied, as shown in Figure 4C. Figure 4D shows static capacitance retention with a strain range from 20% to 40% before the coiled yarn breaks. The coiled supercapacitor exhibits about 84% capacitance retention at the maximum strain of 37.5%. This capacitance drop can be attributed to a linear resistance increase of the coiled electrode when it gets stretched.[29] The inset shows SEM images of microloops before and after 37.5% stretching, showing reversible intercoil distance change.

Based on target applications of power source for wearable electronics, it is necessary to characterize the dynamic electrochemical performance[30] of stretchable supercapacitor by measuring real-time capacitance retention under dynamically applied strain. To guarantee reliable elasticity with negligible residual deformation, the following dynamic characterizations were performed with a moderate strain of 20%.[29] **Figure 5**A–C show dynamically measured CV curves of the coiled supercapacitor with various strain rates. Applied strain rates of 2, 4, and 6% s^{-1} can be converted into frequencies of 0.1, 0.2, and 0.3 Hz for a stretching, respectively, which are close to that of human motion-based movements (0.67–4 Hz).[31] In the static mode, the coiled supercapacitor can retain 90% capacitance at 20% strain and reversibly recovered its initial capacitance when released (**Figure S5**). Therefore, dynamic capacitance variation (capacitance decrease during yarn stretching and recovery during releasing) results in dynamic CV curves with an uneven contour during the tests (Figure 5A–C). Because it takes 10 s for the coiled supercapacitor to reach 20% strain at 2% s^{-1} strain rate (Figure 5A), a single stretching/releasing cycle is included per CV cycle

measured at 100 mV s^{-1} scan rate. Similarly, two and three stretching/releasing cycles are included per CV cycle at 4 and 6% s^{-1} strain rates, respectively (Figure 5B and Figure C). The resulting dynamic capacitance retentions at various strain rates are summarized in Figure 5D. Owing to highly adhesive MnO$_2$ shell formation on the yarn electrode, structural stability, and stable ion supply by the gel electrolyte of the coiled supercapacitor, it exhibits 95.5, 96.2, and 96.3% dynamic capacitance retention at 2, 4, and 6% s^{-1} strain rates without any electrical short-circuit or significant performance degradation.

To characterize the reliability of electrochemical performances of the coiled supercapacitor, repeated stress loading/unloading and charge/discharge cycles were independently conducted. With a moderate strain of 20%, the coiled supercapacitor showed capacitance retentions of 95% after 1000 stretching/releasing cycles and 98.8% after 1000 charge/discharge cycles (**Figure S6**A). Good adhesion between the MnO$_2$ shell and CNT core can be also confirmed through SEM images (Figure S6B). After the cycle tests, the MnO$_2$ shell still remains in a well-attached state over the whole electrode without any observable detachment or cracks. On the other hand, the MnO$_2$ shell deposited onto the smooth surface carbon fiber shows significant detachment after the cycle tests, implying poor adhesion to the electrode (**Figure S7**). This is because the unique surface and internal porosities of twist spun-based CNT yarn[32] have advantages to have good adhesion with active material. Therefore, this simple way for nanoscopic MnO$_2$ deposition effectively provides strong adhesion to the surface of the bare coiled electrode as well as enhancing the energy storage performance without impairing mechanical stretchability or electrochemical cyclability.

In summary, we have reported stretchable and highly performing yarn-based supercapacitors that use unique core–shell-structured coiled electrodes. Pseudocapacitive core(CNT)–shell(MnO$_2$) structured yarns were prepared using an electrochemical method and

the resulting solid-state coiled supercapacitor exhibits high elasticity, specific capacitances, and mechanical, electrochemical cyclabilities. The linear and volumetric capacitances of the coiled supercapacitor were 2.72 mF cm^{-1} and 34.6 F cm^{-3}, respectively. About 84% static capacitance was retained when it was reversibly stretched by 37.5% in strain while 96.3% dynamic capacitance was retained during 20% strain deformation despite the extremely high strain rate of 6% s^{-1}. Owing to the active material's strong adhesion and structural stability of the coiled electrode, the coiled supercapacitor exhibited 95% and 98.8% capacitance retentions after stretching/releasing and charge/discharge cycles, respectively. Because we have deployed the twist–insertion-based coiling method to obtain a highly elastomeric electrode, the presently described supercapacitor fabrication method can be extended to other diverse high-strength monofilament and multifilament polymer fibers (such as polyethylene, Kevlar, silver-plated nylon, polyester, polypropylene, and poly(vinylidene difluoride)) to make supercapacitors that operate at high temperatures and use either hydrophilic or hydrophobic electrolytes.

Experimental Section

CNT forests (~400 μm high and consisting of ~12 nm diameter nanotubes containing ~9 walls) were synthesized using the chemical vapor deposition (CVD) method according to a previous report.[25] Ten layers of 120 mm (length) × 10 mm (width) sized CNT sheets were drawn from the forest and stacked on the glass substrate by ethanol evaporation-based densification. One end of the stacked sheet was connected to the electrical motor for coil twisting. The bare CNT coiled yarn electrodes were fabricated by inserting a giant twist (~50,000 twisting per meter) into CNT sheets. The prepared coiled yarn was electrically connected to 180 μm diameter Cu wire using silver paste for MnO_2 deposition and electrochemical performance characterization. The electrochemical MnO_2 deposition on the pristine CNT coiled yarn was performed using a potentiostatic method of applying 1.3 V (vs Ag/AgCl as reference electrode and Pt mesh as counter electrode) in the three electrode of CHI 627b system (CH Instruments, Austin, TX) in an electrolyte containing 0.02 M $MnSO_4•5H_2O$ and 0.2 M Na_2SO_4 (all chemical products were purchased from Sigma Aldrich). Deposition time for one deposition segment was 3 s and the number of segments was controlled to adjust the deposition amount. The mass of the MnO_2 was measured using EQCM and calculated using the Sauerbrey equation.[33] The PVA–LiCl gel electrolyte was prepared using 3 g PVA (M_w 146,000–186,000) and 6 g LiCl in 30 ml deionized water. The mixture was heated at 90 °C until it became transparent. Two symmetric MnO_2/CNT core–shell structured coiled electrodes were placed in a parallel direction with a small gap (~20 μm) and finally coated with the PVA–LiCl gel electrolyte to complete the fabrication of the coiled supercapacitor. All chemical reagents for solid-electrolyte synthesis were purchased from Sigma Aldrich and used without further processing. To characterize the hybrid core–shell structure of the coiled electrode, cross-sections of the coil were prepared by cutting them

along their diameters using a Ga ion beam (7 nA beam current) in a Focused Ion Beam (FIB, Nova 200) operated at 30 kV. Then, the cut areas were cleaned via Ga ion polishing by etching several micrometers of yarn length with consecutively decreasing ion beam-currents ranging from 5.0 to 0.3 nA. The cleaned-cut yarns were next transferred to a Zeiss Supra 40 SEM to perform the microscopy (at 15 kV) and elemental EDAX mapping analysis (at 20 kV). Clear views of the yarn's cross-sections were attained by orienting the yarn's cut plane parallel to the electron-beam final aperture/detector in the SEM. Other SEM images were obtained by FE-SEM (S4700, Hitachi). The oxidation state of the MnO_2 deposit was characterized by XPS analysis (VG Multilab ESCA 2000 system). All static electrochemical measurements on the coiled supercapacitor utilized a two-electrode configuration with electrochemical analyzer (CHI 627b, CH Instruments). Dynamic CV curves were measured (100 mV s^{-1}) while the coiled supercapacitor was stretched and released at strain rates of 2, 4, and 6% s^{-1} (which can be converted into 180 to 540 mm min^{-1}). A specially constructed machine for applying tensile deformations was used. The length of the supercapacitor was measured using a digital Vernier caliper (500 series, Mitutoyo), which was incorporated into the stretching machine. Stress loading–unloading curves were obtained using a mechanical analyzer (TMA, SS7100). The volumetric capacitance of the coiled supercapacitor was calculated from the CV curves. From $C = I/(dV/dt)$, where I is the discharge current, the single-electrode specific capacitance (C_{sp}) was calculated from the following equation.[1]

$$C_{sp}(F/cm^3) = 4C/Vol_{electrode},$$

where $Vol_{electrode}$ is the total volume of the electrochemical active materials of the two electrodes (MnO_2/CNT coiled electrodes for the present work). In a similar way, total length and surface area of the active materials were used for linear and areal capacitance calculations,

respectively. The factor of 4 comes from the capacitance of the two-electrode system and the combined volume of the two electrodes.[1]

References

[1] J. A. Lee, M. K. Shin, S. H. Kim, H. U. Cho, G. M. Spinks, G. G. Wallace, M. D. Lima, X. Lepro, M. E. Kozlov, R. H. Baughman, S. J. Kim, *Nat. Comm.* **2013**, *4*, 1970.

[2] J. Ren, L. Li, C. Chen, X. Chen, Z. Cai, L. Qiu, Y. Wang, X. Zhu, H. Peng, *Adv. Mater.* **2013**, *25*, 1155.

[3] T. Chen, L. Qiu, Z. Yang, Z. Cai, J. Ren, H. Li, H. Lin, X. Sun, H. Peng, *Angew.Chem. Int. Ed.* **2012**, *51*, 11977.

[4] X. Chen, L. Qiu, J. Ren, G. Guan, H. Lin, Z. Zhang, P. Chen, Y. Wang, H. Peng, *Adv. Mater.* **2013**, *25*, 6436.

[5] H. Sun, X. You, J. Deng, X. Chen, Z. Yang, J. Ren, H. Peng, *Adv. Mater.* **2014**, *26*, 2868.

[6] B. Wang, X. Fang, H. Sun, S. He, J. Ren, Y. Zhang, H. Peng, *Adv. Mater.*, doi:10.1002/adma.201503441

[7] G. Sun, X. Zhang, R. Lin, J. Yang, H. Zhang, P. Chen, *Angew. Chem.* **2015**, *127*, 4734.

[8] Q. Chen, Y. Meng, C. Hu, Y. Zhao, H. Shao, N. Chen, L. Qu, *J. Power Sources* **2014**, *247*, 32.

[9] Y. Meng, Y. Zhao, C. Hu, H. Cheng, Y. Hu, Z. Zhang, G. Shi, L. Qu, *Adv. Mater.* **2013**, *25*, 2326.

[10] J. Bae, Y. J. Park, M. Lee, S. N. Cha, Y. J. Choi, C. S. Lee, J. M. Kim, Z. L. Wang, *Adv. Mater.* **2011**, *23*, 3446.

[11] Y. Ma, P. Li, J. W. Sedloff, X. Zhang, H. Zhang, J. Liu, *ACS Nano* **2015**, *9*, 1352.

[12] Y. Liang, Z. Wang, J. Huang, H. Cheng, F. Zhao, Y. Hu, L. Jiange, L. Qu, *J. Mater. Chem. A*, **2015**, *3*, 2547.

[13] X. Xiao, T. Li, P. Yang, Y. Gao, H. Jin, W. Ni, W. Zhan, X. Zhang, Y. Cao, J. Zhong, L. Gong, W. C. Yen, W. Mai, J. Chen, K. Huo, Y. L. Chueh, Z. L. Wang, J. Zhou, *ACS Nano* **2012**, *6*, 9200.

[14] D. Yu, S. Zhai, W. Jiang, K. Goh, L. Wei ,X. Chen, R. Jiang, Y. Chen, *Adv. Mater.* **2015**, *27,*4895.

[15] Y. Fu, X. Cai, H. Wu, Z. Lv, S. Hou, M. Peng, X. Yu, D. Zou, *Adv. Mater.* **2012**, *24*, 5716.

[16] J. Bae, M. K. Song, Y. J. Park, J. M. Kim, M. Liu, Z. L. Wang, *Angew. Chem. Int. Ed.* **2011**, *50*, 1683.

[17] M. D. Lima, N. Li, M. J. Andrade, S. Fang, J. Oh, G. M. Spinks, M. E. Kozlov, C. S. Haines, D. Suh, J. Foroughi, S. J. Kim, Y. Chen, T. Ware, M. K. Shin, L. D. Machado, A. F. Fonseca, J. D. W. Madden, W. E. Voit, D. S. Galvao, R. H. Baughman, *Science* **2012**, *338*, 928.

[18] C. Yan, J. Wang, W. Kang, M. Cui, X. Wang, C. Y. Foo, K. J. Chee, P. S. Lee, *Adv. Mater.* **2013**, *26*, 2022.

[19] Z. Zhang, J. Deng, X. Li, Z. Yang, S. He, X. Chen, G. Guan, J. Ren, H. Peng, *Adv. Mater.* **2014**, *27*, 356.

[20] Y. Zhang, W. Bai, X. Cheng, J. Ren, W. Weng, P. Chen, X. Fang, Z. Zhang, H. Peng, *Angew. Chem. Int. Ed.* **2014**, *53*, 14564.

[21] C. Choi, S. H. Kim, H. J. Sim, J. A. Lee, A. Y. Choi, Y. T. Kim, X. Lepro, G. M. Spinks, R. H. Baughman, S. J. Kim, *Sci. Rep.* **2015**, *5*, 9387.

[22] P. Xu, T. Gu, Z. Cao, B. Wei, J. Yu, F. Li, J. H. Byun, W. Lu, Q. Li, T. W. Chou, *Adv. Energy Mater.* **2014**, *4*, 1300759.

[23] P. Xu, B. Wei, Z. Cao, J. Zheng, K. Gong, F. Li, J. Yu, Q. Li, W. Lu, J. H. Byun, B. S. Kim, Y. Yan, T. W. Chou, *ACS Nano* **2015**, *9*, 6088.

[24] T. Chen, R. Hao, H. Peng, L. Dai, *Angew. Chem. Int. Ed.* **2015**, *54*, 618.

[25] M. Zhang, K. R. Atkinson, R. H. Baughman, *Science* **2004**, *306*, 1358.

[26] G. Yu, L. Hu, M. Vosgueritchian, H. Wang, X. Xie, J. R. McDonough, X. Cui, Y. Cui, Z. Bao, *Nano Lett.* **2011**, *11*, 2905.

[27] X. Dong, X. Wang, J. Wang, H. Song, X. Li, L. Wang, M. B. Chan-Park, C. M. Li, P. Chen, *Carbon* **2012**, *50*, 4865.

[28] S. W. Lee, J. Kim, S. Chen, P. T. Hammond, Y. Shao-Horn, *ACS Nano* **2010**, *4*, 3889.

[29] Y. Shang, X. He, Y. Li, L. Zhang, Z. Li, C. Ji, E. Shi, P. Li, K. Zhu, Q. Peng, C. Wang, X. Zhang, R. Wang, J. Wei, K. Wang, H. Zhu, D. Wu, A. Cao, *Adv. Mater.* **2012**, *24*, 2896.

[30] X. Li, T. Gu, B. Wei, *Nano Lett.* **2012**, *12*, 6366.

[31] S. Jung, J. Lee, T. Hyeon, M. Lee, D. H. Kim, *Adv. Mater.* **2014**, *26*, 6329.

[32] C. Choi, J. A. Lee, A. Y. Choi, Y. T. Kim, X. Lepro, M. D. Lima, R. H. Baughman, S. J. Kim, *Adv. Mater.* **2014**, *26*, 2059.

[33] S. L. Kuo, N. L. Wu, *J. Electrochem. Soc.* **2006**, *153*, A1317.

Figure Captions

Figure 1. Overview SEM image of (A) MnO_2/CNT core–shell structured coiled electrode (scale bar = 50 μm). Its magnified surface images of (B) before (scale bar = 1 μm) and (C) after MnO_2 deposition onto the bare coiled yarn (scale bar = 400 nm). Uniaxially aligned bare CNT electrode's surface is covered by mesoporous and nanoscopic MnO_2 film after deposition, constructing a core(CNT)–shell(MnO_2) structured yarn electrode. Cross-sectional SEM images of (D) MnO_2/CNT coiled yarn electrode (scale bar = 20 μm) and (E) magnification of the edge part indicated by a square in D (scale bar = 3 μm). The MnO_2 shell is denoted by arrows. Volume and weight ratio of MnO_2 shell to total coiled electrode are calculated to be 4.9% and 17.2%, respectively.

Figure 2. Elemental mapping analysis performed on the coil cross-section area and the location of (A) C (carbon, red dots), (B) O (oxygen, green dots), and (C) Mn (manganese, blue dots) atoms are spotted. (D) XPS analysis on MnO_2 shell. The binding energy difference between the Mn 2p doublet peaks is 11.8 eV, which corresponds to that expected for MnO_2.[21]

Figure 3. (A) Schematic illustration for the complete solid-state coiled supercapacitor, which comprises two symmetric MnO_2/CNT core–shell coiled electrodes and gel electrolyte. (B) CV curve comparison before and after MnO_2 deposition onto the bare coiled yarn. As a consequence of the pseudocapacitive contribution of the nanoscopic MnO_2 shell, the CV area increased by about 512% after MnO_2 deposition. (C) CV curves of solid-state coiled supercapacitor measured from 10 to 100 mV s^{-1} scan rates. (D) Nyquist curve shows a low ESR value of 0.07 Ω cm^{-3} around a high frequency of 100 kHz (inset) and vertical line. (E) Calculated volumetric and linear capacitances of solid-state coiled supercapacitor for various

scan rates. The highest volumetric and linear capacitances (based on the dimensions of both MnO$_2$/CNT coiled electrodes) are 34.6 F cm^{-3} and 2.72 mF cm^{-1} at 10 mV s^{-1} scan rate, respectively.

Figure 4. (A) Optical images of solid-state coiled supercapacitor before and after application of 37.5% tensile strain. The initial length of as-used coiled supercapacitor is 16.8 mm for the stretching test. Inset shows magnified coiled supercapacitor, which was assembled using two parallel coiled electrodes with a constant gap (~20 μm gap, scale bar = 100 μm). (B) Stress loading/unloading curves of the hybrid MnO$_2$/CNT coiled electrode with tensile strains from 20% to 40%. (C) Static CV curve comparison before (black line) and after 37.5% strain applied (red line) to the coiled supercapacitor, showing 84% capacitance retention. (D) Capacitance retention versus static strain. The inset shows magnified SEM images of microloops before and after 37.5% strain applied (scale bar = 50 μm).

Figure 5. Dynamically measured CV curves (at 100 mV s^{-1} scan rate) during 20% strain stretching/releasing cycles with various strain rates. Nonstretched ($\varepsilon = 0$) coiled supercapacitor's CV curves are denoted for comparison (black line), while the dynamically measured CV curves with strain rates of (A) 2% s^{-1} (green line, 10 s for full stretching), (B) 4% s^{-1} (blue line, 5 s for full stretching), and (C) 6% s^{-1} (red line, 3.3 s for full stretching) are presented. (D) Overall dynamic capacitance retentions of a coiled supercapacitor, showing 95.5%, 96.2%, and 96.3% retentions at 2, 4, and 6% s^{-1} strain rates, respectively, after three charge/discharge cycles.
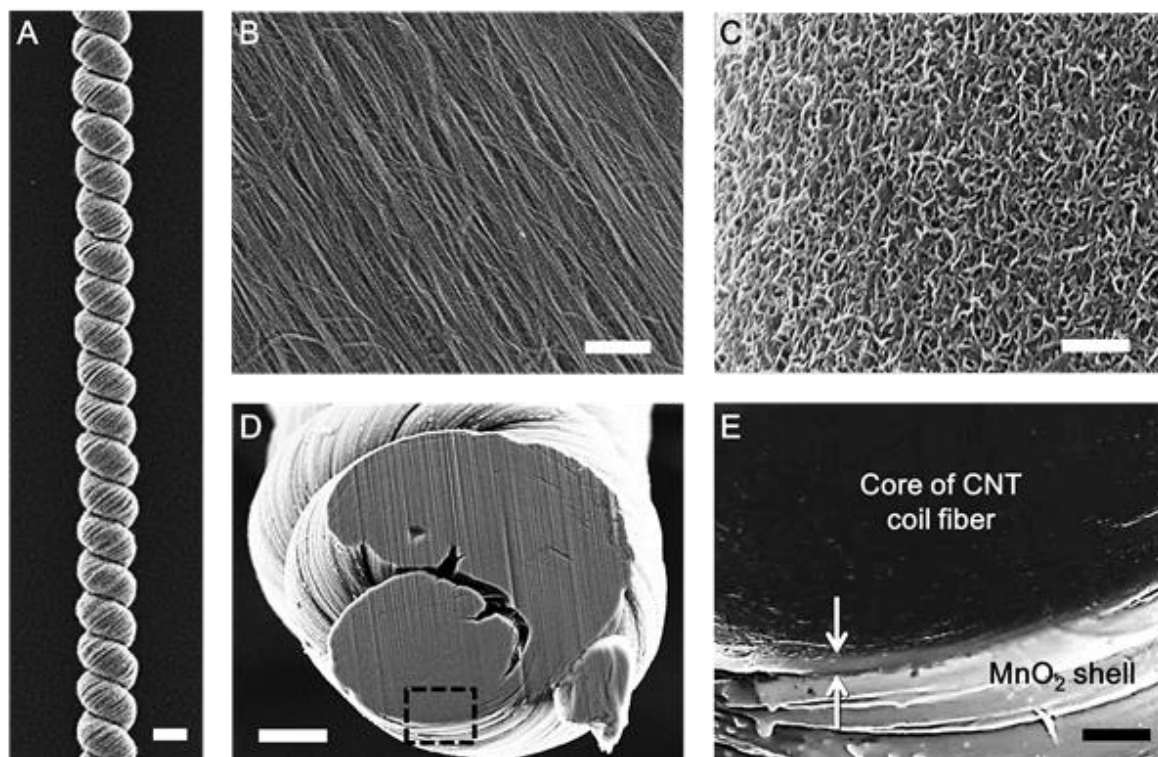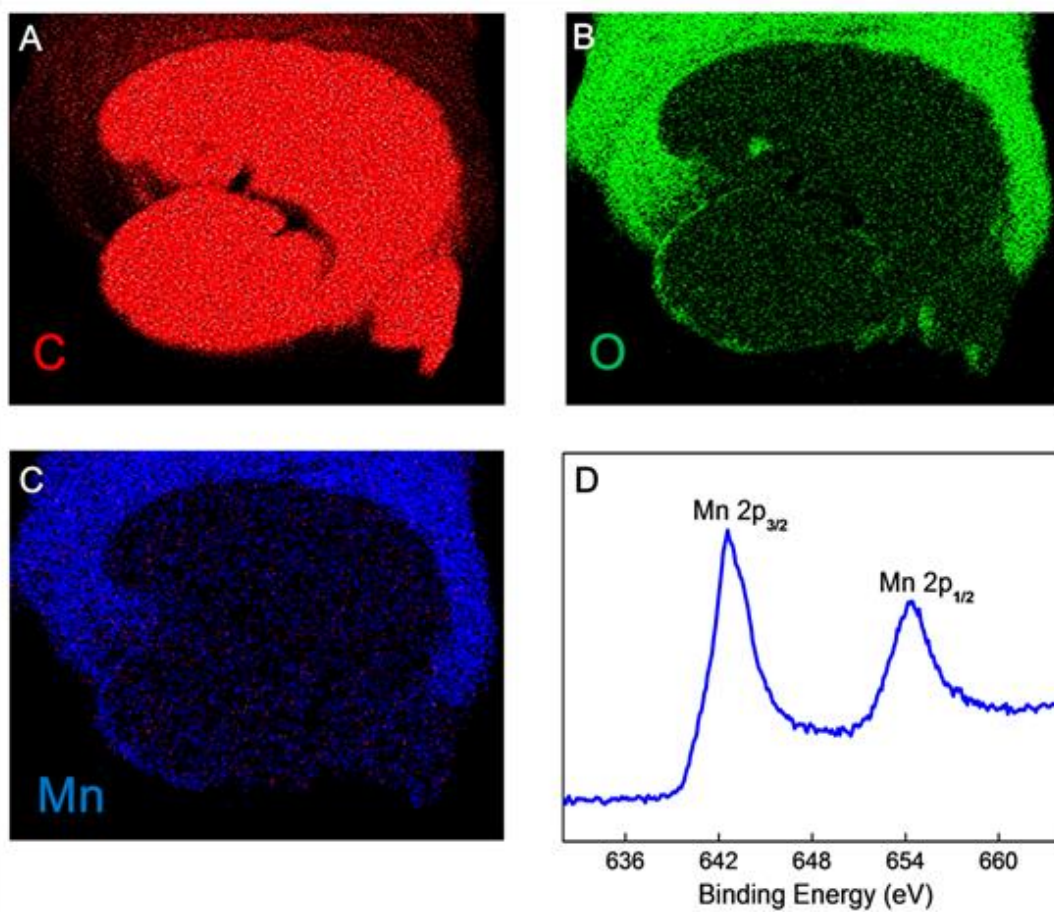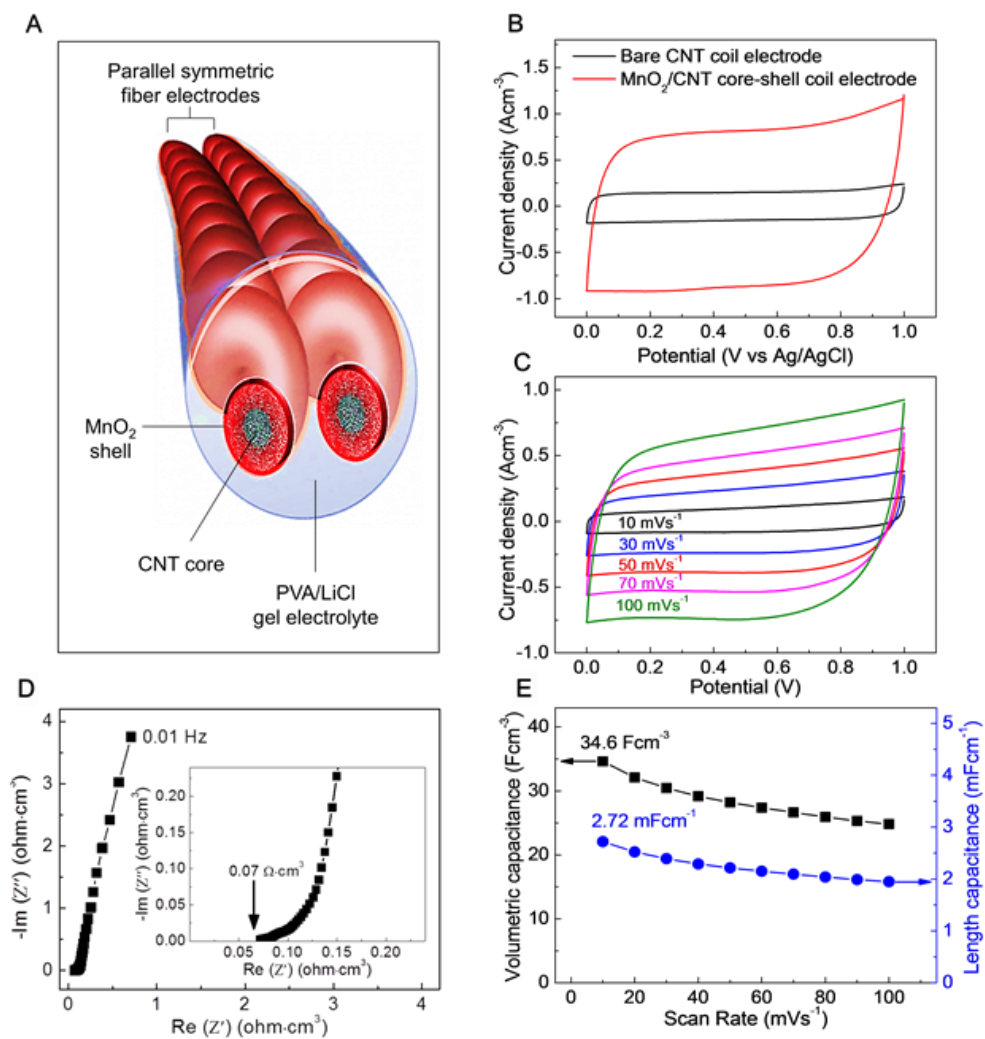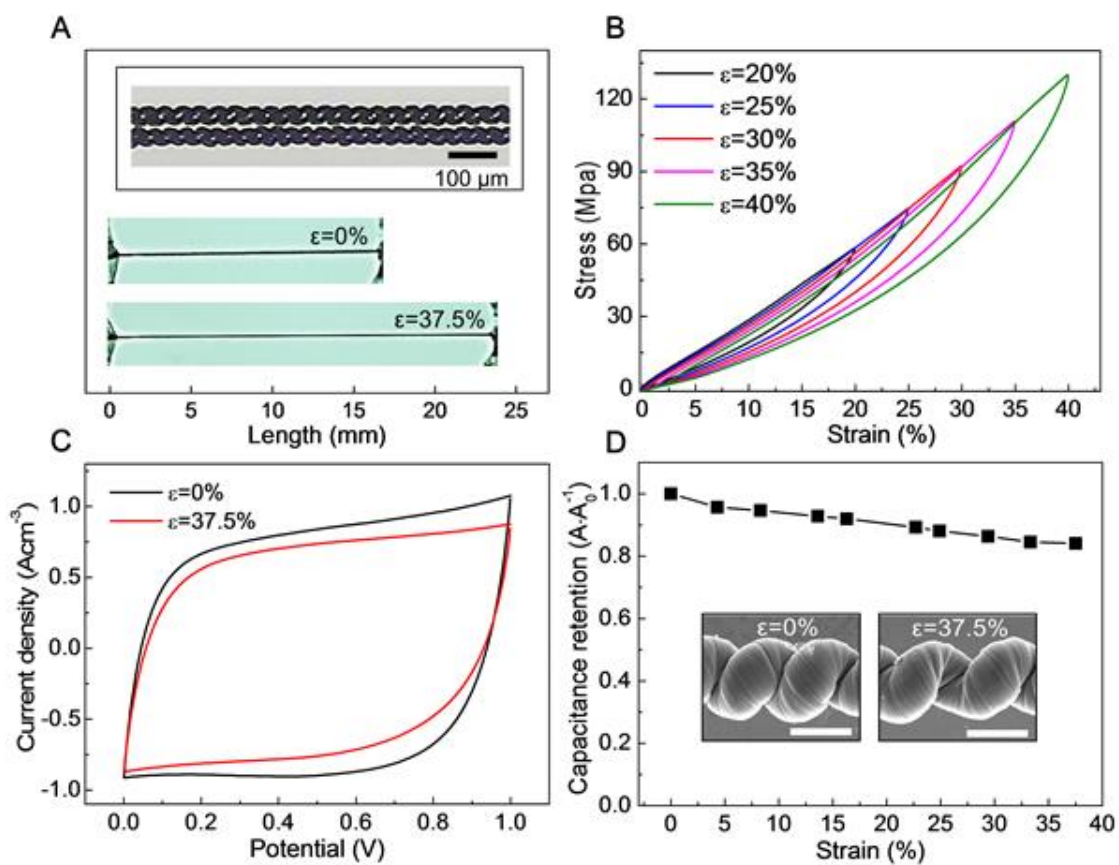
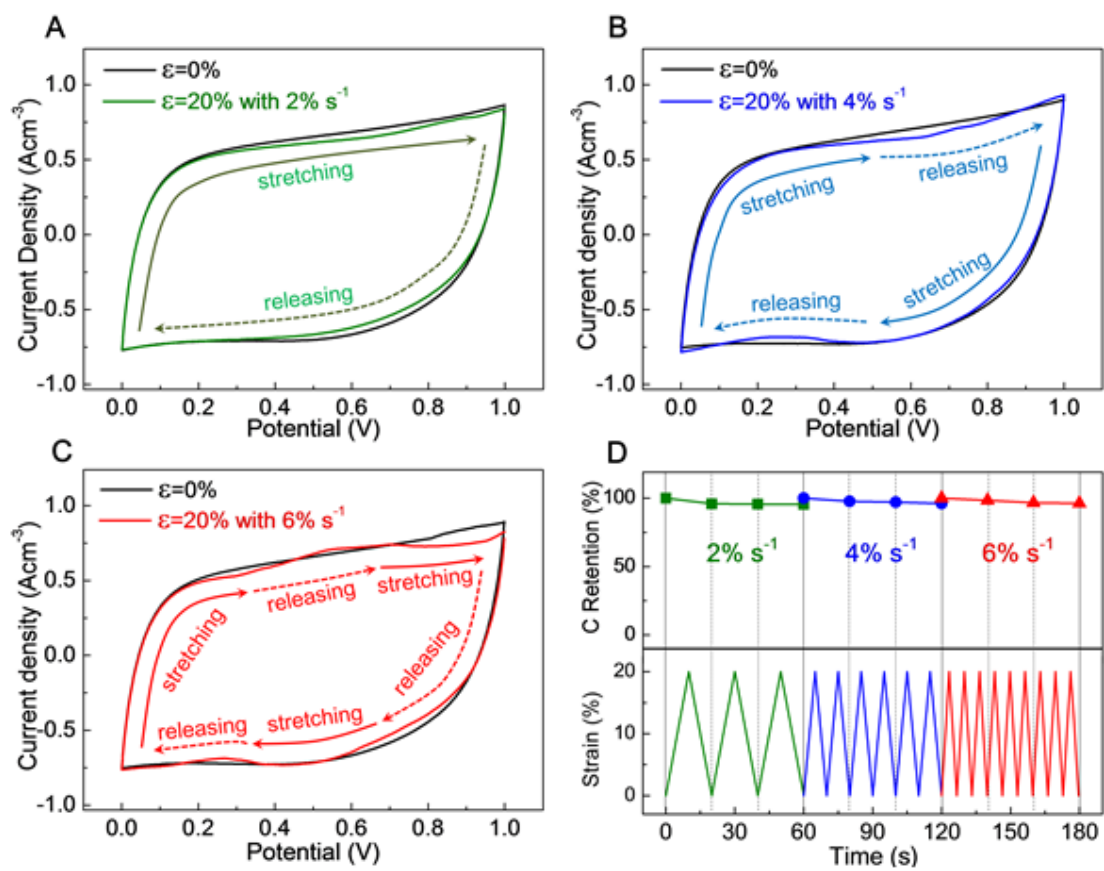**Figure 1**

Figure 2

Figure 3

Figure 4

Figure 5

Table 1. Specific capacitance comparison of the coiled supercapacitor with reported FBSs.

Deformability	Electrode Materials (Ref. No.)	C_L [mF cm^{-1}]	C_A [mF cm^{-2}]	Condition
Stretchability	MnO$_2$/CNT coiled fiber (Present Work)	2.72	61.25	CV[a] at 10 mV s^{-1}
	CNT spring fiber (24)	0.51	27.07	GCD[b] GCD at 424 μA cm^{-2}
	Buckled MnO$_2$/CNT fiber (23)	0.26	27.98	CV at 10 mV s^{-1}
	All graphene core–sheath fiber (9)	0.02	1.7	CV at 50 mV s^{-1}
Flexibility	MnO$_2$/CNT fiber (2)	0.019	3.57	GCD at 0.5 μA
	MnO$_2$/ZnO nanowires/polymer fiber (16)	0.02	2.4	CV at 100 mV s^{-1}
	Graphene fiber (8)	0.01	0.72	GCD at 424 μA cm^{-2}
	TiO$_2$/CNT fiber (3)	0.024	0.6	GCD at 0.25 μA
	CNT fiber, CNT film (4)	0.029	8.66	GCD at 1 μA
	PEDOT/CNT fiber (1)	0.47	73	CV at 10 mV s–1
	Graphene/CNT fiber (5)	0.027	4.97	GCD at 0.04 A g^{-1}
	ZnO nanowire/graphene fiber (10)	0.025	0.4	CV at 100 mV s^{-1}
	Pen ink/carbon, metal fiber (15)	1.008	26.4	CV at 100 mV s^{-1}

[a] Cyclic voltammograms (CV). [b] Galvanostatic charge–discharge test (GCD).